

# Surprising results from a detailed simulation of a common envelope phase

AN AMR STUDY OF THE COMMON-ENVELOPE PHASE OF BINARY EVOLUTION

written by

PAUL M. RICKER<sup>1</sup> AND RONALD E. TAAM<sup>2,3</sup>

<sup>1</sup> Department of Astronomy, University of Illinois at Urbana-Champaign, Urbana, IL, USA; pmricker@illinois.edu

<sup>2</sup> Department of Physics and Astronomy, Northwestern University, 2131 Tech Drive, Evanston, IL, 60208, USA; r-taam@northwestern.edu

Expert in parallel numerical simulations and binary stars

Received 2011 July 19; accepted 2012 January 22; published 2012 June 25

Accepted by: ApJ; editor: D. De Jong

ABSTRACT

This paper presents the first three-dimensional hydrodynamical simulation of the common-envelope

Expert in hydrodynamical simulations and close binaries

over 40 refereed papers on common envelope evolution

TL;DR:

A hydrodynamical simulation of the common-envelope phase of a red giant star and its companion shows that:

Gravitational drag dominates the inspiral & the Bondi-Hoyle-Lyttleton prescription drastically overestimates accretion.

The hydrodynamic evolution of the common-envelope (CE) phase of a low-mass binary composed of a  $1.05 M_{\odot}$  red giant and a  $0.6 M_{\odot}$  companion has been followed by the orbits of the system using a high-resolution method in three spatial dimensions. During the rapid inspiral phase, the interaction of the companion with the red giant's extended atmosphere leads to significant energy loss, continuing to be lost at the end of the inspiral. In the subsequent phase of orbital decay, momentum and energy reduces the orbital separation by a factor of seven. After this inspiral phase the eccentricity of the orbit rapidly decreases with time. The gravitational drag dominates hydrodynamic drag at all times in the evolution, and the commonly used Bondi-Hoyle-Lyttleton (BHL) prescription for accretion onto the companion significantly overestimates the rate. In spite of the orbital decay, the gas flow in the orbital plane in the vicinity of the two cores is subsonic without gas nearly corotating with the red giant core and circulating about the red giant companion. The gas is primarily ejected from the system and is scattered within  $30^\circ$  of the orbital plane, and the spiral shocks in this material leave an imprint on the density and velocity structure. Of the energy released by the inspiral of the cores, only about 25% goes toward ejection of the envelope.

**Key words:** binaries: close – hydrodynamics – methods: numerical – stars: winds, outflows

**Online-only material:** color figures

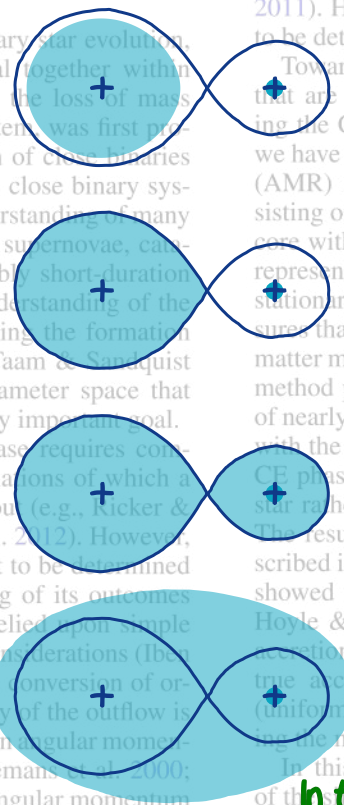
## What is a common envelope?

### 1. INTRODUCTION

It is a very short-lived period in the life of some binary stars during which the two stars orbit inside a single shared gas envelope.

This can occur during dynamically unstable Roche-Lobe overflow. An example of this is a giant branch star as it often undergoes unstable mass transfer.

This is how unstable Roche-Lobe overflow can lead to a common envelope.



## Why is a common-envelope interesting?

2010; Ge et al. 2010; Deloye & Taam 2010; Loveridge et al. 2011). However, the physical mechanism(s) involved remains to be determined.

Toward the goal of understanding the physical mechanisms that are important in governing the ejection of material during the CE phase and the formation of the compact remnant, we have carried out a high-resolution adaptive mesh refinement (AMR) simulation of the evolution of a binary consisting of a  $1.05 M_{\odot}$  red giant star containing a  $0.36 M_{\odot}$  degenerate core with a  $0.6 M_{\odot}$  companion. The use of AMR in this study represents a major improvement over previous work based on stationary nested grid calculations (Taam et al. 1998). This method ensures that the deep interior of the CE is always well resolved as matter moves about the center of mass of the system. The method permits one to study systems with binary components of nearly equal masses, which could not be adequately modeled with the stationary nested grid.

Because common-envelopes are dominated by fast, non-linear fluid dynamics, computationally intensive hydrodynamical simulations are required to understand these systems.

In this paper we examine the intermediate time evolution of the system. The early stages were described in Paper I. Here, we focus specific attention on the determination of the drag force on the red giant star and the resulting mass ejection from the system. To gain a deeper understanding of the importance of the interaction of the core of the red giant and its companion, we also simulate the case of a binary consisting of two stars of

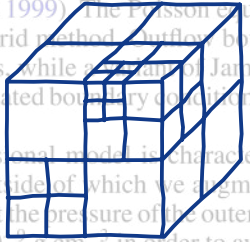
component and the accretion onto each component. In addition, we examine the orbital decay of the system and the matter ejected from the Eddington rate, providing additional evidence that a system has passed through this stage, independent of the outcome. Section 2 briefly details the numerical methods and simulation parameters. The results are presented in Section 3, and we conclude with a discussion of their implications in the last section.

## 2. METHODS

**Ricker & Taam simulated a 1.05 solar mass red giant star using a one-dimensional stellar structure code. It contains a 0.69 solar mass gaseous envelope and a 0.36 solar mass solid core.**

**They analyse its properties and compare the results with common assumptions and previous simulations.**

**They interpolate the properties of the model onto a special 3-dimensional grid of blocks called an octree**



The one-dimensional model is characterized by a radius of  $2.2 \times 10^{12}$  cm, outside of which we augment it with a uniform ambient medium at the pressure of the outermost layer of the star and a density of  $10^{-6}$  g cm $^{-3}$  in order to avoid artificial outflow associated with inadequate resolution of the outermost layers. Within a box of size  $1.1 \times 1.1 \times 1.1$  cm per  $10^{12}$  cm $^3$  blocks, we use four levels of refinement to achieve a smallest zone spacing of  $2 \times 10^{10}$  cm. The innermost  $0.36 M_{\odot}$  ( $6 \times 10^{10}$  cm) of the gas in the red giant star is replaced by a spherically symmetric  $6 \times 10^{10}$  cm $^3$  of particles moving in a circular orbit around the star. The resulting three-dimensional model is allowed to relax for one dynamical time (12 days). The relaxation stage is applied to the gas velocities at the end of each time step, beginning with 0.9 and gradually reducing the amount of damping by increasing the factor toward unity. By the end of the relaxation stage the typical velocities are less than  $2 \text{ km s}^{-1}$ .

**A 0.6 solar mass companion is introduced to the octree, moving in a circular orbit in the gaseous envelope.**

**Then, they start the hydrodynamical simulation using a new method called AMR.**

**AMR or adaptive mesh refinement dynamically subdivides sensitive or turbulent regions of the octree into smaller cubes. This improves precision while keeping the simulation efficient!**

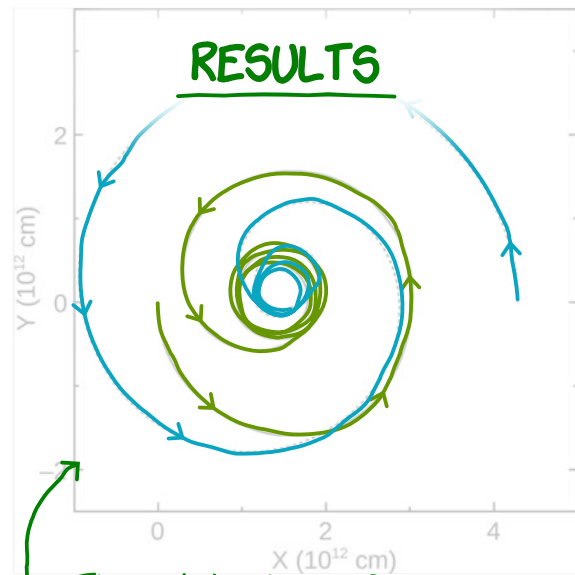


Figure 1. Orbital trajectories. Shown are the orbital evolution of the binary system during the initial phase of the collapse of the CFe binary system.

**The orbits shrink from a period of approximately 50 days to a period of 5 days. The orbits also become more circular.**

Applications and ending with the Ranger cluster at the Texas Advanced Computing Center. Using the Teragrid service unit conversion calculator, we estimate the cost of the run up to 56.7 days of simulation time to be the equivalent of 512 cores for 792,000 core hours on Ranger.

This is caused by two drag effects. The description of the early evolution of the CFe binary was briefly presented in Paper I. Here, we report on the further evolution of the system during which envelope stripping accelerates and the orbital separation decreases. The orbital separation has been reduced by a factor of seven, primarily because of the gravitational drag. In the next section we discuss the intermediate evolution beginning at this point.

**1. Hydrodynamical drag**

The evolution of the system described in the previous section has continued through 56.7 days of simulation time. Figures 1 and 2 illustrate the orbital trajectories and orbital separation of the stars, respectively. The gravitational interaction between the two stars has resulted in a decrease in the orbital period from its initial value of 1.5 months to less than five days. By comparing the time between periastron and subsequent apastron to the time from apastron to subsequent periastron, it can be seen that the orbit continues to evolve. However, the orbital evolution timescale has become significantly longer than it was during the early inspiral between 27 and 41 days. In fact, the timescale of orbital decay has increased from  $\sim 5.5$  days. The orbit is also gradually becoming more circular; its eccentricity at 36.7 days is  $\sim 0.05$ . The orbital separation of  $\sim 1.1 \times 10^{12}$  cm is larger than the spacing zone spacing  $\Delta r \approx 1.0 \times 10^{12}$  cm, the size of the star. In order to determine the contribution of the gravitational drag and hydrodynamic drag acting on the red giant core and the companion star during the orbital decay phase, we illustrate their variation as a function of time in Figure 3. The hydrodynamic drag force is computed using the control-surface

**2. Gravitational drag**

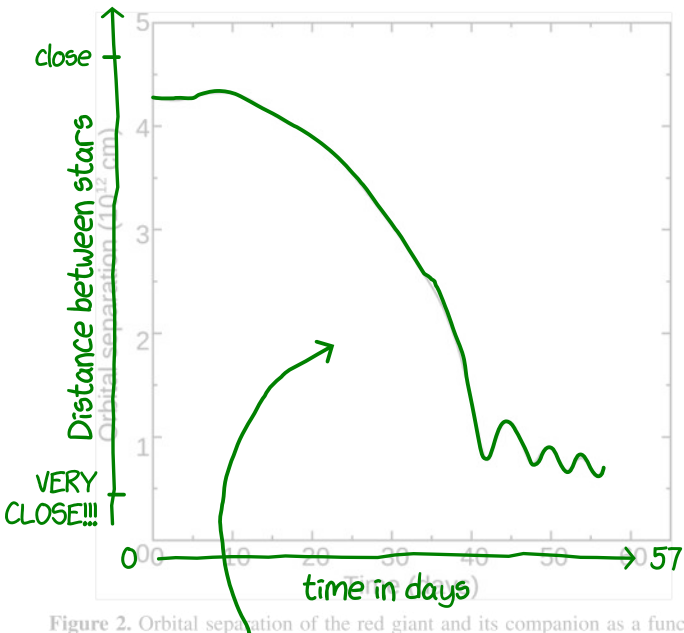
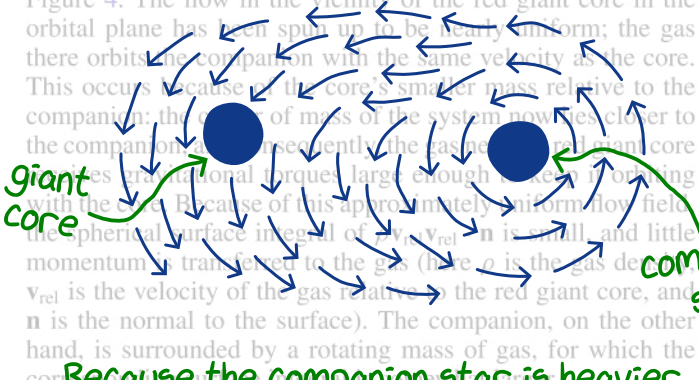


Figure 2. Orbital separation of the red giant and its companion as a function of time.

The distance between the stars in the common envelope decreases quickly during the early evolution, and continues to decrease afterwards.

As for the early stages of CE evolution, the gravitational drag force for both stellar cores continues to exceed the hydrodynamic drag force by more than an order of magnitude. The main culprit turns out to be the gravitational drag force on the particles relative to the gas. The gravitational force on the particles is due to the two stellar cores. As the cores spiral together, the gravitational drag force on the red giant core is initially about a factor of five less than that on the companion star because of its central location within the envelope, but as gas expands to greater radii and the two cores spiral together, they start to experience the same gravitational drag force.

The hydrodynamical drag force differs for the two cores. This happens because the gas in the envelope behaves differently around both cores.



Because the companion star is heavier than the giant core, the gas circles around the companion star, while it moves uniformly with the giant core.

### 3.2. Core Accretion

Therefore, the hydrodynamical drag is larger for the companion star.

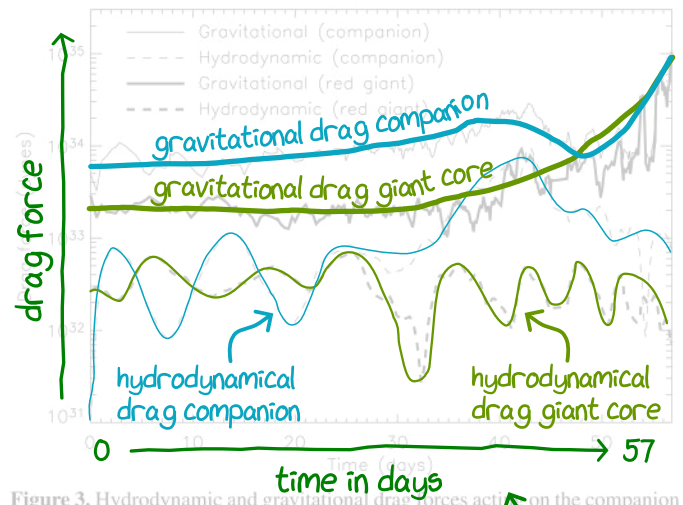


Figure 3. Hydrodynamic and gravitational drag forces act on the companion star and red giant during the inspiral phase of the CE binary system. Force values have been boxcar smoothed over five time steps.

mass flux through a spherical control surface and integrating this flux over time. Since we do not attempt to model the accretion process itself, as this would require a much higher resolution than we are able to achieve, the radius of the control surface is taken as a free parameter. The choice of this radius should be larger than the spatial resolution to ensure convergence and to avoid Cartesian grid effects, but it should also be smaller than the spatial scale length of the gas density field to avoid including gas elements that are not taking part in the accretion process. Furthermore, the radius of the control surface is adopted such that the ratio of the gravity of the accretor to the gravitational factor after the accretion event,  $\text{grav} / \text{grav}_{\text{core}}$ , is unity. This ratio is determined for a given stellar core and control surface radius  $R_{\text{acc}}$  by choosing  $N = 32(R_{\text{acc}}/\Delta x)^2$  uniformly distributed points on a sphere of this radius centered on the core's location. The gas density and velocity fields (relative to the core's velocity) are linearly interpolated from the AMR grid onto these points, and the flux is determined via

$$M = \rho \mathbf{v}_{\text{rel}} \cdot \mathbf{n} dA \approx \frac{2\pi^2 R_{\text{acc}}^2}{N} \sum_{i=1}^N \rho_i \mathbf{v}_{\text{rel},i} \cdot \mathbf{n}_i \sin \theta_i, \quad (1)$$

where the integral is taken over the control surface,  $\theta_i$  is the polar angle of the  $i$ th sample point, and  $\mathbf{v}_{\text{rel}}$  is the relative velocity of the core and the gas. Note that the control surface radii chosen here are the mean points all lie within a highly refined region of space and

This is INTERESTING!!  
The domination of the

gravitational drag over the hydrodynamical drag suggests we might have been overestimating the amount of mass that gets accreted. Let's look into this!

We have performed this calculation for both stellar cores using control surface radii of  $1.4 \times 10^{11}$  and  $2.1 \times 10^{11}$  cm (5–10.5 zones). The results presented here are displayed as a variation of mass as a function of evolution time. For comparison, we also show the mass accretion to be expected if the accretion rate were set by the standard BH prescription. In general, the BH prediction is  $\sim 100$  times the actual rate of mass accreted, as was found for the early-inspiral phase in Paper I.

Our results suggest that the larger choices for control surface radii ( $1.4$  and  $2.1 \times 10^{11}$  cm) overestimate the accretion radius as they likely incorporate too much of the cores' surroundings to provide a reliable mass accretion estimate. In addition to the disagreement with the results for the smaller control surface radii, these choices yield time intervals in which the accreted mass decreases, suggesting that the gravity of the individual cores is not the dominant determinant of the gas dynamics

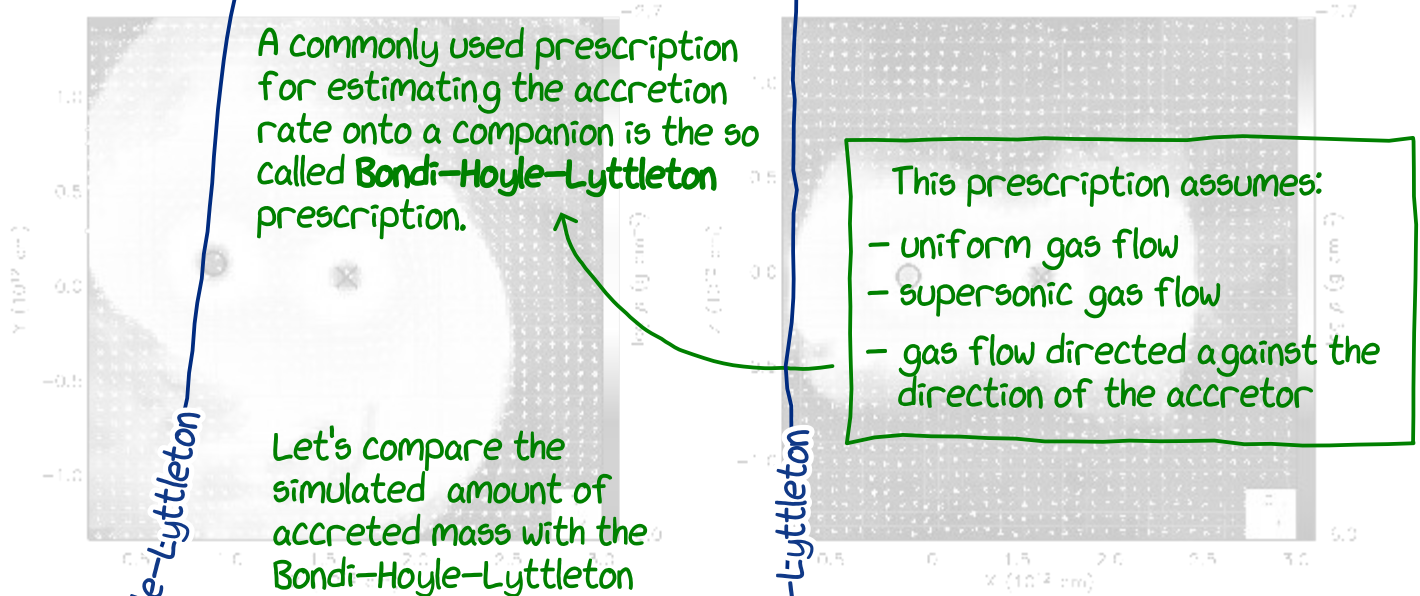


Figure 4. Left: density distributions for the companion star. Right: density distributions for the red giant core. The orbital plane is shown for the orbital period  $T = 56.7$  days. The location of the companion star ( $x$ ) and red giant core ( $y$ ) are shown. As for the left panel, the axes are in units of  $10^2$  cm. A color version of this figure is available in the electronic edition.

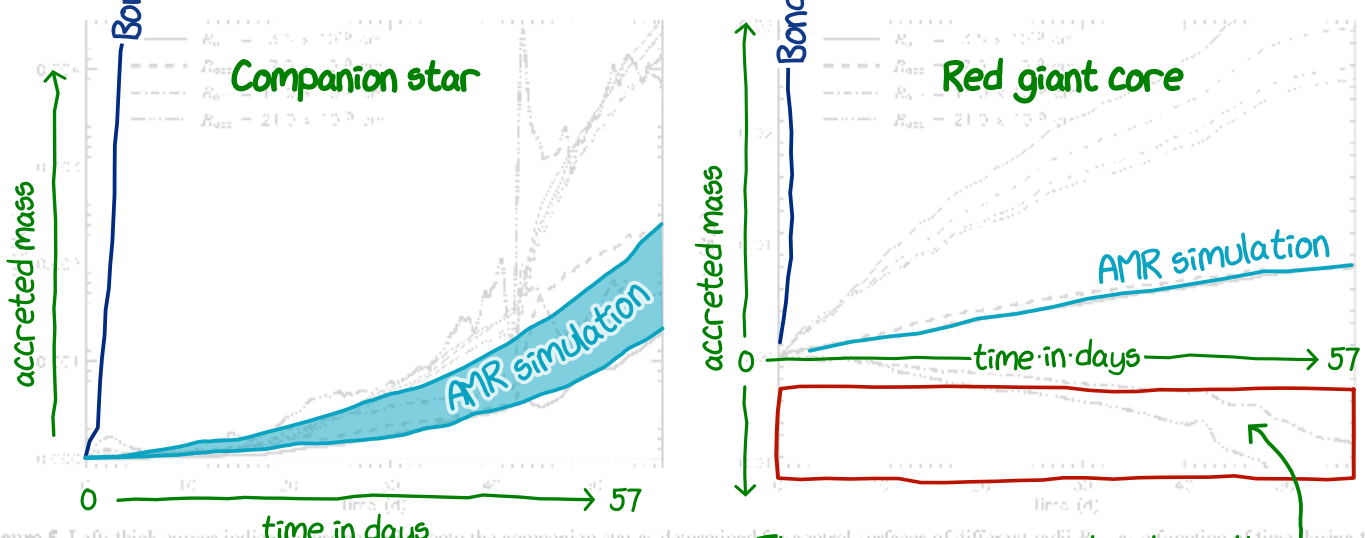


Figure 5. Left: thick curves indicate the simulated accretion rate onto the companion star as determined from the AMR simulation during the inspiral phase of the CE binary system. Thin curves show the accreted mass as determined using the BHL model with different radii and different flow velocities within the same control surfaces, divided by 100. Right: same as the left panel, except for the red giant core.

in regions of these extents. The fact that the accreted mass decreases over time is consistent with the prediction. This is consistent with the fact that the companion's mass is greater than that of the red giant, and the radius of influence is larger. The two models agree well for the first 10 days, they differ by a factor of two for the companion. For the companion, the average accretion rate over the first 57 days of the beginning of the simulation is  $\sim 10^{-2} M_{\odot} \text{ yr}^{-1}$ , while the higher gas density in the vicinity of the red giant core yields a larger estimate,  $\sim 6 \times 10^{-2} M_{\odot} \text{ yr}^{-1}$ .

The BHL accretion rate is derived under the assumption that the gas flow is uniform, supersonic, and directed against the accretor's direction of travel. We can understand the differences between our results and the BHL prediction by examining the flow field in the orbital plane around the red giant core.

**WOW! It seems like the commonly used Bondi–Hoyle–Lyttleton prediction MASSIVELY (100x) overestimates the amount of mass that gets accreted.**

and the Companion (Figures 4 and 6). At late times the flow is subsonic and the flow is subsonic in the BHL prediction, although the flow is subsonic in the vicinity of both cores, but for each the flow field is such as to yield a low accumulation rate (uniform across the red giant core, circular about the companion). Thus, the assumptions underlying the BHL prediction do not hold during the evolution of this system.

Note that since the gas density is not uniform within the accretion control surface (it varies by an order of magnitude or so), it might be argued that a BHL rate computed using density, pressure, and velocity values very close to the cores is unrepresentative of the conditions in their vicinity. However, our results for BHL accretion rates are based on averages within the same control surfaces as used for estimating the actual accretion rate. The difference in the BHL accretion rate encountered in using different averaging radii is much smaller than the

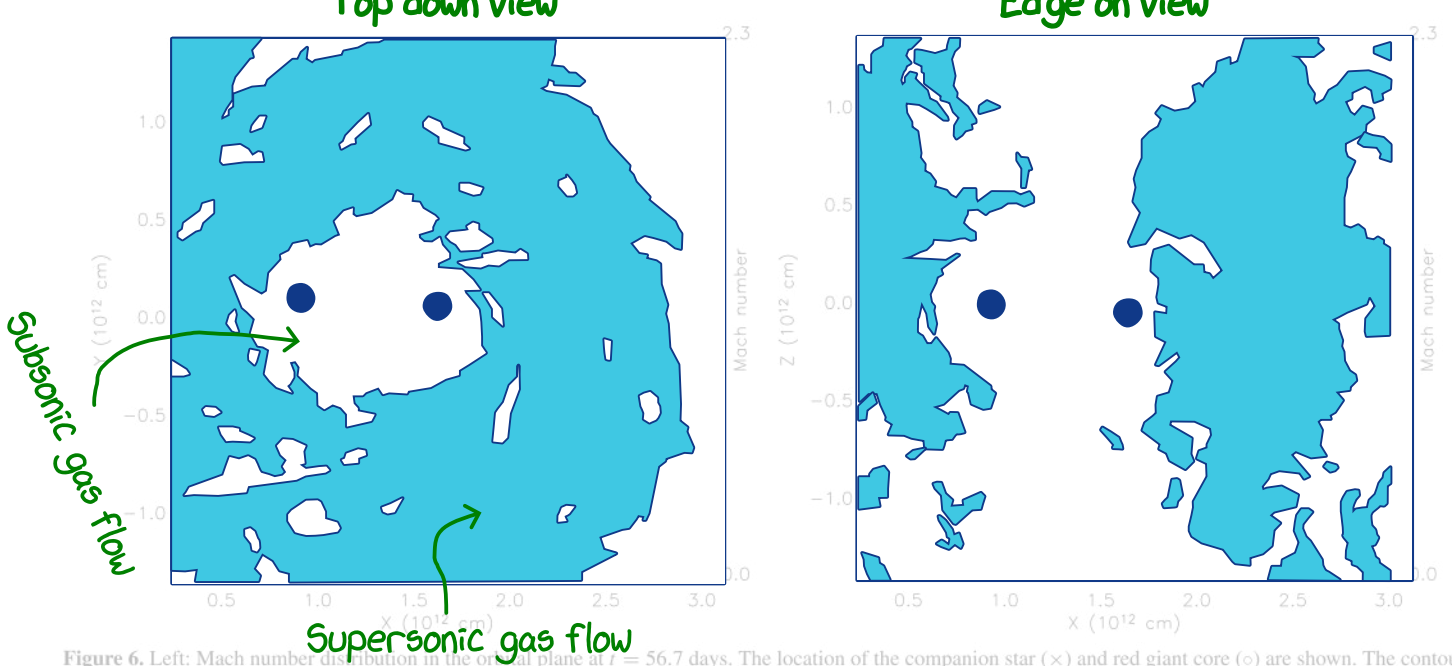


Figure 6. Left: Mach number distribution in the orbital plane at  $t = 56.7$  days. The location of the companion star ( $\times$ ) and red giant core ( $\circ$ ) are shown. The contour indicates the transition from subsonic to supersonic flow. Right: as for the plot on the left, but for the  $xz$ -plane.

(A color version of this figure is available in the online journal.)

difference between the BHL rates and the values obtained using Equation (1). (Note that the BHL rate curves have been divided by 100 to fit them within the figure.)

### 3.3 Outflow

The angular momentum transported from the orbital motion to the envelope should be conserved in the outflow. Regardless of the outcome of the CE phase (merger or stabilization as a close binary), and the complete ejection of the envelope the core should contract to the pre-white dwarf stage, evolving to higher effective temperatures in the process. If the core is sufficiently massive, the effective temperatures will be sufficiently high to lead to the formation of a planetary nebula. In a seminal study, Balick (1987) suggested that the interaction of a fast stellar wind from the central star with the envelope in certain circumstances may give rise to asymmetric planetary nebulae with an elliptical or “butterfly” morphology. Although the specific model that we have adopted here contains a low-mass helium degenerate core and will not produce a planetary nebula, the morphology of the outflowing matter from our simulation is generic to outflows resulting from the CE phase (see Taam et al. 2009). The properties of the outflow of the envelope is another important aspect of the common-envelope phase!

Besides accretion and changes to the binary orbit, outflow of the gaseous envelope is another important aspect of the common-envelope phase! Most of the envelope mass is concentrated in a roughly spherical ball around the centre.

Figure 8 illustrates the angle-averaged gas density in the orbital plane as a function of radius for several different times between 31.8 and 56.7 days. One can clearly see the expansion of the envelope material with time. Behind the expanding envelope

**Close to the cores, the gas moves subsonically!**

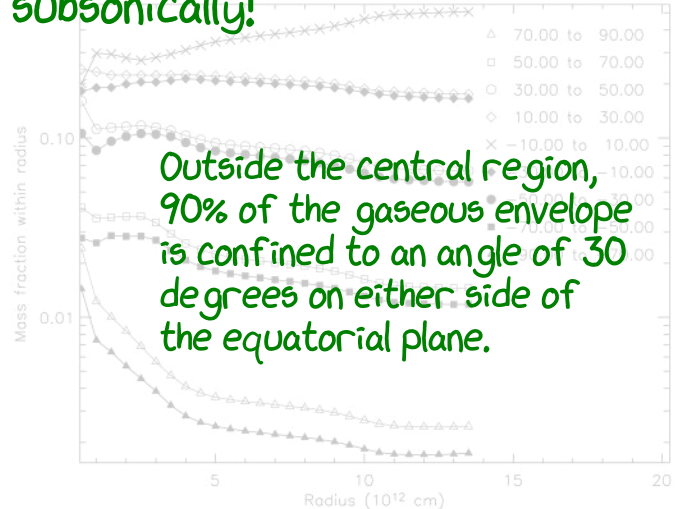


Figure 7. Enclosed mass vs. radius for gas lying in different polar angle bins, as measured using the point  $(1.5 \times 10^{12} \text{ cm}, 0, 0)$  as origin and the Cartesian  $z$ -axis as the polar  $z$ -axis, at  $t = 56.7$  days.

for the outflow, the gas density adopts a roughly  $r^{-5/3}$  profile. This density slope is intermediate between the expectations for constant-velocity isotropic and planar winds, which given the equatorial dominance suggests that the outflow velocity must increase with radius. The mass loss leads to the ejection of  $0.18 M_{\odot}$  of the CE as seen in Figure 9, where the amount of unbound mass is illustrated as a function of time. The rate of mass loss after about 45 days is nearly constant and at the end of the simulation is  $\sim 2 M_{\odot} \text{ yr}^{-1}$ . The simulation clearly shows that the envelope expands.

From Figure 4, when plotting the distribution of gas in the orbital ( $xy$ ) plane and  $xz$ -plane at  $t = 56.7$  days, it can be seen that within a radius of about  $10^{12} \text{ cm}$ , there is no evidence of shock structure, and the gas Mach number is less than one (see Figure 6). This suggests that the angular momentum is removed from the central regions by tidal torques rather than spiral shocks as seen in simulations with larger mass ratios (see

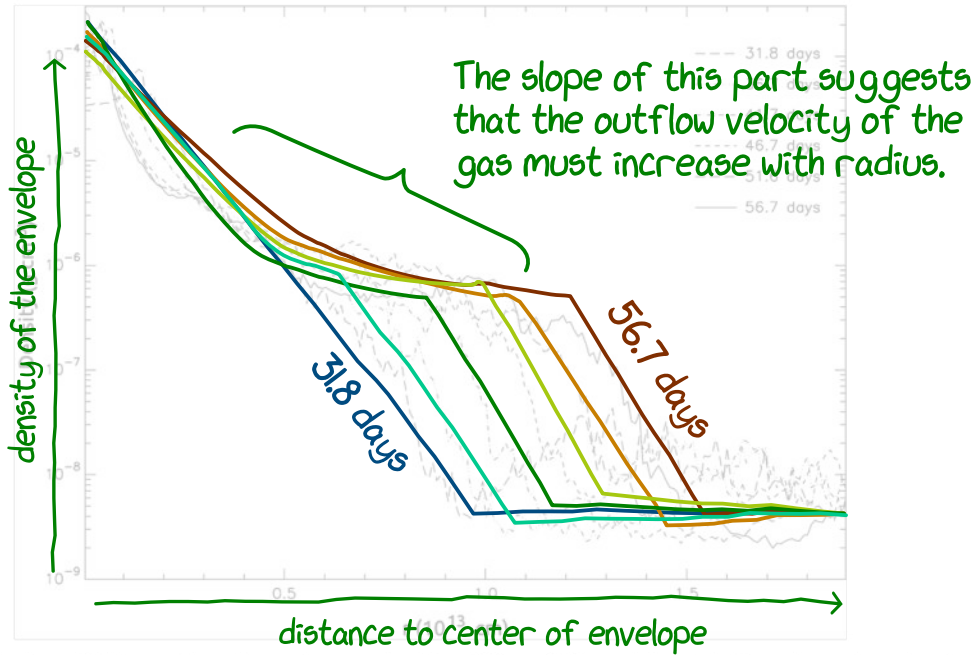


Figure 8. Angle-averaged gas density profile in the orbital plane, using the point  $(1.5 \times 10^{12} \text{ cm}, 0, 0)$  as origin and the Cartesian  $z$ -axis as the polar  $z$ -axis, at different times.

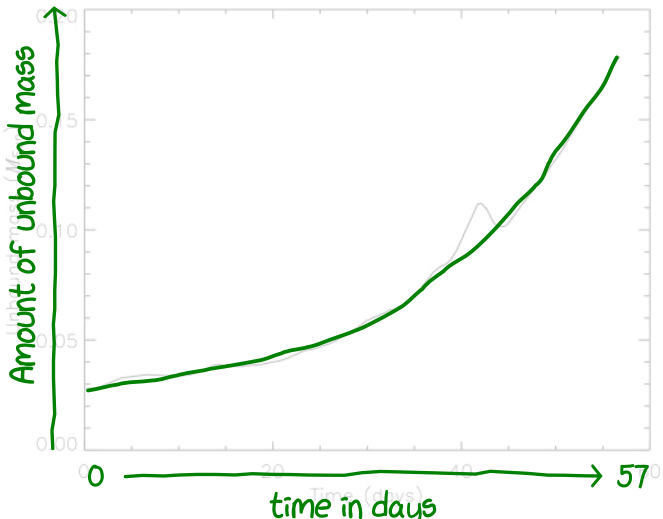


Figure 9. Unbound gas mass as a function of time.

Sandquist et al. 1998). At larger radii, however, trailing spiral features are in fact seen (Figure 10). By examining the variation of gas quantities in the envelope around the center of mass, we can establish and quantify the nature of these features. Figure 11 shows the variation of gas density, pressure, and radial and tangential velocity components along a line in the orbital plane originating at the point  $(-1.5 \times 10^{12} \text{ cm}, 0, 0)$  and describing a  $\sim 10^5$  g cm $^{-3}$  orbit. This figure clearly shows that the rate of mass loss becomes nearly constant after about 45 days. At least four features of decreasing strength are identified as the radius increases. Each feature corresponds to an orbit of the binary following the initial inspiral.

**During the simulated evolution, the envelope ejects 0.18 solar masses of gas.**

**The rate of mass loss becomes nearly constant after about 45 days.**

**At the end of the simulation, the mass loss rate is about 2 solar masses per year.**

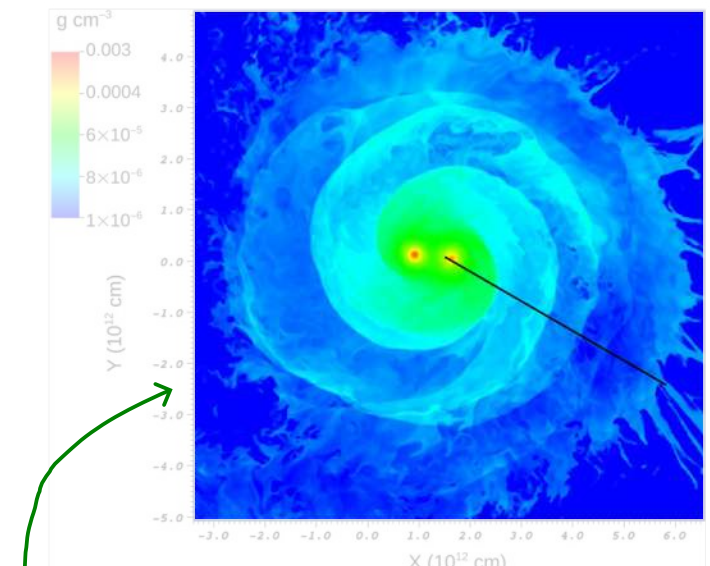


Figure 10. Gas density in the orbital plane on large scales at  $t = 56.7$  days. Gas quantities sampled at  $t = 56.7$  days. (A color version of this figure is available in the online journal.)

**Enjoy this pretty picture! It shows the density of the common-envelope. You can clearly see the spiral structure and regions with great jumps in colour. These are shocks!**

effects of CE evolution. We can estimate the required unbinding energy by looking at the total energy (kinetic + thermal + potential) profiles for the initial relaxed system with the companion and red giant spin aligned (but before any binary evolution). As the binary evolves, we can track the change in the total bound gas mass from the beginning to the end of the simulation, giving the binding energy of the system and by the stars' interaction. Assuming that this unbound mass is stripped from the outer layers of the red giant, we use the mass and energy profiles to find the unbinding energy by subtracting the enclosed energy at the radius at which the binned energy becomes negative.

**If you look closely, you can see at least 4 shocks.**

**Each one corresponds to an orbit of the binary during the inspiral**

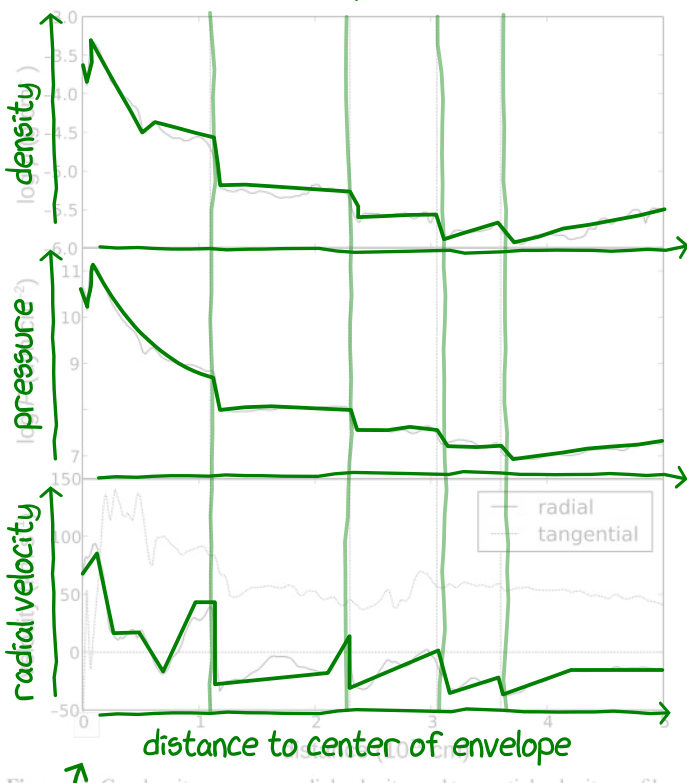


Figure 1. Gas density, pressure, radial velocity, and tangential velocity profiles along the line indicated in Figure 10 at  $t = 56.7$  days. Vertical dotted lines indicate locations of spiral shocks.

We find that in the initial conditions only  $0.66 M_{\odot}$  of the envelope is bound (mass coordinate  $3 R_{\odot}$ ), while the remaining  $0.34 M_{\odot}$  is unbound due to the orbital motion of the red giant. We include this remaining amount in our estimate of the unbound mass, but not in the calculation of the efficiency (we can perform the latter by considering only the bound material). At  $t = 56.7$  days,  $0.51 M_{\odot}$  of the envelope remains bound. The initial enclosed energies corresponding to enclosed masses of  $0.66$  and  $0.51 M_{\odot}$  are  $-1.3 \times 10^{47}$  erg and  $-1.1 \times 10^{47}$  erg, respectively, so the energy needed to unbind the remaining  $0.15 M_{\odot}$  that is lost is  $\sim 2 \times 10^{46}$  erg.

At the end of the simulation the  $0.51 M_{\odot}$  of the envelope that remains bound has an energy of  $-4.6 \times 10^{46}$  erg, so its energy has also increased. The increase in energy of the bound material (gas + cores) decreases along the mesh potential as measured at each point in the center, and about the self-potential of the envelope. The total energy released by the inspiralling material is  $\sim 8 \times 10^{46}$  erg, which is roughly consistent with what we expect from the decrease in orbital radius (the difference is due to the gravitational field of the gas). The cores' kinetic energy increases by  $2.2 \times 10^{46}$  erg. Thus, the total energy released by the inspiralling cores is  $\sim 8 \times 10^{46}$  erg. Of this amount, 75% goes into raising the energy of the part of the envelope that remains bound, while the remaining 25% goes into unbinding  $0.15$  solar masses of gas.

## Conclusions & Discussion

We have used a large AMR simulation to study the CE evolution of a binary system initially consisting of a  $1.05 M_{\odot}$  red giant with a  $0.36 M_{\odot}$  degenerate core and a  $0.6 M_{\odot}$  companion. The use of AMR allows us to simulate stellar pairs with mass

ratio close to unity at high resolution. We have followed the system through 57 days of evolution, during which time it has experienced several spiral-in events between orbital radii of  $7$  to  $8 R_{\odot}$ . The envelope fraction steadily decreases with time to a value of  $0.08$ . The CE interaction has led to the loss of  $0.15 M_{\odot}$  of the red giant's initial gaseous envelope at this point in time. We note that this fraction of unbound mass is larger than in the work by Sandquist et al. (2009), perhaps because of the higher initial mass ratio (companion to the red giant) of the system. **0.18 solar mass, or 26% of gas became unbound. This is larger than a previous study, but consistent with theoretical trends.**

Based on the decrease in orbital radius, the efficiency of the mass ejection is  $\sim 25\%$ . Given that the mass-loss rate from the system is  $\sim 2 M_{\odot} \text{ yr}^{-1}$ , the remaining mass is expected to be removed within two additional months (comparable to the orbital period). The orbital decay will continue until the envelope is removed. Additional orbital decay will result in the ejection of the remaining envelope. It is possible that ejected material will fall back onto the stars, but this matter may fall back, and the effect of any material surrounding the system in the form of a circumbinary disk (Kashi & Soker 2011) may lead to further orbital decay. It is likely that the system will survive the CE phase with an orbital period of less than three days.

**The system will likely survive the common-envelope phase with a period of less than 3 days.**

A number of studies concerning the early stages of the evolution of this model system, the gravitational drag acting on the two stellar cores due to the nonsymmetrical gas distribution dominates over the hydrodynamical drag. The flow pattern in the vicinity of the stellar cores is nearly uniform in the red giant core and irregular for the companion, and in both cases it is subsonic. Such a description of the flow renders the hydrodynamical drag simple estimates of the drag based on a BHL prescription suspect and should be noted when considering evolutionary calculations of lower dimensionality.

The commonly used BHL prescription for estimating the mass accretion rate onto the companion overestimates the actual accretion rate by nearly two orders of magnitude. As discussed in Papaloizou & Pringle (1977), the BHL model is unlikely to be able to predict the outcome of the inspiralling of a neutron star in a stellar envelope to a black hole. We note, however, that the BHL model is not the only one that can be used to model the mass accretion rate. The results that we infer from our calculations can still exceed the rate for hypercritical accretion ( $\sim 10^{-3} M_{\odot} \text{ yr}^{-1}$ ; Chevalier 1993) suggesting that the outcome of the accretion evolution of an inspiralling neutron star is dependent on the evolutionary state of its giant companion.

An alternative prescription for the CE drag and resulting inspiral has been proposed by Meier & Meyer-Hofmeister (1979; MM), who consider a model for the CE evolution of a  $5 M_{\odot}$  red giant and a  $1 M_{\odot}$  main-sequence star. In this model, the systems is treated as a two-star system with the two stars being frictionally interacting with a outer envelope undergoing differential rotation. The angular momentum transfer and energy dissipation in the envelope is due to the tidal forces. Because the tidal drag is neglected, the system becomes more compact. Because the tidal drag appears to be the dominant dissipation mechanism in our calculation, we would argue that at least during the rapid inspiral phase the MM model greatly underestimates the drag and hence overestimates the inspiral timescale (see their Figure 5). Moreover, the radially averaged specific entropy profile of our system at  $t = 56.7$  days

is convectively stable, so if convective turbulence should have developed but did not because of our resolution, its integral scale and hence the size of the scale length would be smaller than our minimum zone spacing ( $7 \times 10^{10}$  cm). The mixing length in MM is of order the physical scale length which in our calculation is  $\sim 7 \times 10^{10}$  cm, so the mixing length is correspondingly overestimated in their model. In our Figure 4, it is clear that the velocity field in the central regions is laminar on these scales. Instead, angular momentum is removed from the envelope interior regions by spiral shocks.

## HOWEVER

**The model is not perfect!**

**It is possible that turbulence should exist in these regions but is missing due to physics not included in the simulation.**

It is conceivable that our simulation could help to invert the entropy gradient and thus drive turbulence on small scales, changing the nature of the angular momentum transport. If the gas is ionized, its radiation pressure, but the gas is treated as being fully ionized, so energy derived from recombination is not included. In significant amounts of recombination in the inner regions, it could both raise the entropy there and contribute to the ejection of more envelope material. However, a rough estimate of the optical depth due to electron scattering (which dominates at the temperatures present in the inner regions) shows that gas and radiation pressure are dominant at a radius of  $5 \times 10^{12}$  cm. Thus recombination photons are important only in the very outer regions of the envelope and not in the inner region where the star is located. For example, the energy from recombination is not included. Enough recombination could raise the entropy in the inner regions and cause turbulence.

Luckily for us, electron scattering (which dominates at this regime) only becomes important at large radii, and thus, recombination should not be important in the inner region.

**For larger red giants however, recombination can no longer simply be ignored.**

It might be possible to detect systems that recently underwent a common-envelope phase by looking at the spectral lines emitted by the gas.

**The lines might show jumps!**

a large number of stars, or spectroscopic follow-up of optical transients detected in a large-area photometric survey with a high cadence (such as LSST).

We acknowledge helpful conversations with Ronald Webbink, Orsola de Marco, and Jean-Claude Passy, as well as useful comments by the anonymous referee. Partial support for this work has been provided by NSF through grants AST-0200876 and AST-0703950. Computational work was carried out using NSF Teragrid resources at the National Center for Supercomputing Applications (NCSA) and the Texas Advanced Computing Center (TACC) under allocations TG-AST040024 and TG-AST040034N. P.M.R. acknowledges the Kavli Institute for Theoretical Physics, where some of this work was performed with funding by NSF under grant PHY05-51164 (the report number for this paper is NSF-KITP-11-085). FLASH was developed and is maintained largely by the DOE-supported Flash Center for Computational Science at the University of Chicago.

## Acknowledgements

## REFERENCES

- Balick, B. 1987, *AJ*, 94, 671
- Bondi, H. 1952, *MNRAS*, 112, 195
- Bondi, H., & Hoyle, F. 1944, *MNRAS*, 104, 273
- Chevalier, R. A. 1993, *ApJ*, 411, L33
- Colella, P., & Glaz, H. M. 1985, *J. Comput. Phys.*, 59, 264
- Colella, P., & Woodward, P. R. 1984, *J. Comput. Phys.*, 54, 174
- Deloye, C. J., & Taam, R. E. 2010, *ApJ*, 719, L28
- Eggleton, P. P. 1971, *MNRAS*, 151, 351
- Eggleton, P. P. 1972, *MNRAS*, 156, 361
- Fryxell, B., Olson, K., Ricker, P., et al. 2000, *ApJS*, 131, 273
- Ge, H., Webbink, R. F., Han, Z., & Chen, X. 2010, *Ap&SS*, 329, 243
- Hoyle, F., & Lyttleton, R. A. 1939, *Proc. Camb. Phil. Soc.*, 34, 405
- Iben, I., Jr., & Tutukov, A. V. 1985, *ApJS*, 58, 661
- James, R. A. 1977, *J. Comput. Phys.*, 25, 71
- Kashi, A., & Soker, N. 2011, *MNRAS*, 417, 1466
- Loveridge, A. J., van der Sluys, M., & Kalogera, V. 2011, *ApJ*, 743, 49
- Massarotti, A., Latham, D., Sosza, D., & Fogel, J. 2008, *AJ*, 135, 209
- Meyer, F., & Meyer-Hofmeister, E. 1979, *ApJ*, 238, 167
- Nelemans, G., & Tout, C. A. 2005, *MNRAS*, 356, 753
- Nelemans, G., Verbunt, F., Yungelson, L. R., & Portegies Zwart, S. F. 2000, *A&A*, 360, 1011
- Paczynski, B. 1976, in IAU Symp. 73, Structure and Evolution of Close Binary Systems, ed. P. Eggleton, S. Mitton, & J. Whelan (Dordrecht: Reidel), 75
- Passy, J.-C., De Marco, O., Fryer, C. L., et al. 2012, *ApJ*, 744, 52
- Ricker, P. M., & Taam, R. E. 2008, *ApJ*, 672, L41
- Sandquist, E. L., Taam, R. E., & Burkert, A. 2000, *ApJ*, 533, 984
- Sandquist, E. L., Taam, R. E., Chen, X., Bodenheimer, P., & Burkert, A. 1998, *ApJ*, 500, 909
- Taam, R. E., & Ricker, P. M. 2010, *New Astron. Rev.*, 54, 65
- Taam, R. E., & Sandquist, E. L. 2000, *ARA&A*, 38, 113
- Timmes, F. X., & Arnett, D. 1999, *ApJS*, 125, 277
- Xu, X.-J., & Li, X.-D. 2010, *ApJ*, 716, 114

## Citations